

Coupling of Graphene Plasmonics Modes Induced by Near-Field Perturbation at Terahertz Frequencies

Wei Wei^{1,2,3} · Jinpeng Nong^{1,2} · Linlong Tang³ · Yong Zhu^{1,2} · Haofei Shi^{3,4}

Received: 26 July 2015 / Accepted: 26 November 2015 / Published online: 10 December 2015
© Springer Science+Business Media New York 2015

Abstract The coupling between graphene surface plasmonic (GSP) modes and evanescent wave modes induced by near-field perturbation is investigated systematically in the grating-spacer-graphene hybrid system. Simulation results show that the near-field perturbation due to a small change of the geometrical structure disturbs the coupling characteristics, leading to the evolution of the absorption spectra and the spatial energy redistribution of GSP modes. By exploring the physical mechanism, the shift of the resonant absorption frequency can be quantified through the variation of the effective permittivity around graphene, while the first order evanescent wave in the grating plays a fundamental role in determining the absorbance in the coupling process. Further discussion indicates that the different penetration abilities of GSP wave into dielectric and metal grating contribute to the discrepancy of the energy distribution of GSP modes. Our study provides new physical insight and promotes a further step for the design of plasmonics devices at terahertz frequencies.

Keywords Graphene · Coupling · Surface plasmons · Near-field perturbation · Terahertz frequencies

Introduction

Plasmonics at terahertz (THz) frequencies has sparked a wealth of research interest driven by its capabilities of enhancing near-field effects, improving imaging resolution and making nonlinear interactions effective [1–3]. These features render it promising for developing the next-generation nanophotonics devices in THz bio-sensing, ultra-high resolution imaging, and ultrafast communications fields [4–6]. In such an explosion of interesting fields, classic metallic nanostructures [7–9] play a pivotal role in controlling and manipulating the terahertz electromagnetic wave at scales substantially smaller than its wavelength. However, at terahertz frequencies, plasmon on metal surface suffers great losses and limited tunability, severely hindering the development of THz plasmonic devices.

Graphene that emerged as a fascinating two-dimensional atomic film with extraordinary electrical and optical properties, opens up a brand-new opportunity to address these challenges [10, 11]. As a kind of revolutionary plasmonics material, graphene supports intrinsic transverse-magnetic (TM) plasmon modes with extremely tight confinement, relatively long lifetime, and very low losses, making it possible to manipulate the THz electromagnetic wave in the single atomic plane. In particular, its plasmon frequencies can be tuned electrically [12], which offers an innovative solution to break through the bottlenecks of the conventional terahertz devices. These unprecedented properties point to a promising future of graphene as an ideal platform for carbon-based optoelectronics across the THz spectrum region. Very recently, great progresses have been made on the investigation of the basic

✉ Wei Wei
wwwei@cqu.edu.cn

Haofei Shi
shi@cigit.ac.cn

¹ Key Laboratory of Optoelectronic Technology and Systems, Ministry of Education of China, Chongqing University, Chongqing 400044, China

² College of Optoelectronic Engineering, Chongqing University, Chongqing 400044, China

³ Chongqing Institute of Green and Intelligent Technology, Chinese Academy of Sciences, Chongqing 401122, China

⁴ Chongqing Engineering Research Center of Graphene Film Manufacturing, Chongqing 401329, China

characteristics of graphene surface plasmonics (GSP) modes. For instance, the GSP eigenmode is predicted theoretically and observed experimentally [13–15]. The excitations of GSP wave are demonstrated in both patterned graphene (graphene nano-disks [16], micro-ring [17], micro-ribbon [18], and anti-dot arrays [19]) and continuous graphene film (based on prism configuration [20] and diffraction grating [21–23]). And the distinctive propagation characteristics of GSP wave have been implemented for designing various optical switch [18], interferometer [24], optical waveguide [25], directional coupler [26], and so forth.

However, previous researches mainly focus on the physical nature, excitation, and propagation of the GSP modes, further investigation about the effect of near-field perturbation on the coupling of GSP modes remains unrevealed, which is an inevitable problem when designing an active plasmonics device [27]. For a classic dielectric-graphene-dielectric plasmonics system [13], a small change in the geometric structure of the periodical nanostructure will yield a perturbation within the near-field region, which certainly affects the coupling between GSP modes and evanescent wave modes in the nanostructure, leading to a considerable variation of absorbance spectra and mode patterns of the system. Thus, it raises interesting and urgent questions: how the near-field perturbation influences the performance of the system and what is the underlying mechanism behind this effect? Understanding these working principles will play a fundamental role in building basic blocks for the development of the GSP-based THz devices and systems.

Herein, we explore the coupling effect of GSP modes induced by near-field perturbation in one-dimensional grating-spacer-graphene hybrid systems. First, the influence of the near-field perturbation on the coupling between GSP modes and evanescent wave modes in dielectric and metallic hybrid systems are investigated systematically. Then, the physical mechanism behind the coupling effect is revealed using effective medium theory and rigorous coupled wave theory. Finally, the penetration of GSP waves into the dielectric and metallic gratings is also discussed in detail. Our study may promote innovative methods for confining and controlling terahertz wave and provide fundamental insight for the designs of plasmonics devices at terahertz frequencies, such as ultrasensitive terahertz biosensor, ultrafast terahertz modulators, and super-resolution imaging.

Structure and Results

As schematically depicted in Fig. 1, the grating-spacer-graphene hybrid systems are proposed to investigate the coupling of GSP modes induced by near-field perturbation. In order to systematically investigate the coupling behaviors in the hybrid systems, the systems are categorized into the

dielectric grating-spacer-graphene (DGSG) hybrid system and the metallic grating-spacer-graphene (MGSG) hybrid system considering the different permittivity characteristics of the dielectric grating ($Re(\epsilon) > 0$) and metallic grating ($Re(\epsilon) < 0$), as shown in Fig. 1a, c, respectively.

The grating contains the following geometric parameters: period Λ , height h , and occupation ratio η . A dielectric spacer with thickness of t is sandwiched between grating and graphene, which can be employed to eliminate the non-uniform doping and strains of the graphene induced by the grating. Without explicit statement, the permittivity of dielectric grating and spacer used for calculations are assumed to be $\epsilon_r = 11.8$ and $\epsilon_2 = 2.25$. The permittivity of metal (Au) is given by the Drude model [28]. Graphene is modeled as a monolayer with thickness of 0.34 nm. Simulations are carried out by finite element method employing *Comsol mutiphysics*. The mesh size inside graphene layer along the Z-axis is 0.03 nm, and the mesh size gradually increases outside the graphene.

As a transverse magnetic (TM) wave irradiates vertically from the top of the grating, it will be scattered into various diffraction orders which are evanescent waves. Once the in-plane wavevector of a GSP wave matches the wavevector of a diffraction order, these two kinds of evanescent waves couple together to excite a highly confined fundamental GSP mode in graphene as illustrated in Fig. 1b. The coupling strength is determined by the overlap area between a GSP mode and an evanescent wave mode [29]. In such process, the variation of distance t between grating and graphene and the change of the occupation ratio η of grating will yield near-field perturbation to the coupling of GSP modes. This leads to the variation of the overlap area, and consequently, the energy exchange between GSP modes and evanescent wave modes, which results in the changes of the essential features in GSP modes. These features are characterized by the evolution of the absorption curves in the spectral domain and the energy redistribution of GSP modes in the spatial domain. Therefore, to investigate systematically, the effect of near-field perturbation caused by the variation of t and η on GSP modes, the resonant frequency, absorbance, and spatial mode patterns are calculated and compared in the DGSG and MGSG hybrid systems, respectively.

Coupling of GSP Modes Induced by Perturbation in Dielectric Nanostructure

In this section, the coupling effect of the GSP modes induced by near-field perturbation as t decreases is investigated. Figure 2a illustrates the evolution of the absorption spectra of the DGSG hybrid system when the occupation ratio and the period of the grating are fixed as $\eta = 50\%$ and $\Lambda = 200$ nm. Once the wavevector matching condition is satisfied, the normal-incidence free space light is coupled into GSP wave and highly confined in graphene. Then, a characteristic absorption

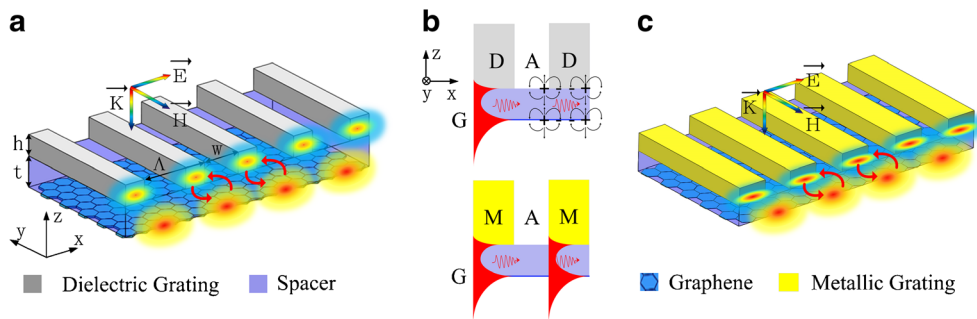


Fig. 1 Schematic of the DGSG hybrid system (a) and the MSGS hybrid system (c). The gray and yellow regions are dielectric grating and metallic grating whose period, height, and groove width are Δ , h , and w , respectively. The violet region is a dielectric spacer with thickness of t ,

and under the spacer is a monolayer graphene. **b** The cross section of the hybrid system shows the physical process of the coupling between GSP modes and evanescent wave modes

peak can be observed in the absorption spectrum, and the incident light is converted into GSP wave with maximum excitation efficiency at the resonant frequency. As t decreases from 45 to 5 nm, the resonant frequency of GSP wave redshifts from 17.72 to 13.93 THz, along with the increase of absorbance from 7.25 to 41.97 % due to the enhanced coupling between GSP modes and evanescent wave modes in the grating. It means that the coupling strength can be modulated by the thickness of the spacer.

The near-field perturbation also impacts the spatial energy distribution of GSP modes in this process. To visually observe the energy redistribution, the GSP mode patterns are simulated with a fixed frequency of 15 THz when t equals 45, 35, 15, and 0 nm, respectively. As indicated in Fig. 2b, energy of GSP

modes redistributes in the sub-wavelength region, exhibiting a concentration of GSP energy from the grating gap toward the grating ridge as the dielectric grating gets close to the graphene layer. To further illustrate this tendency, the near-field normalized $|E_x|$ intensity along the graphene layer is extracted from Fig. 2b and depicted in Fig. 2c. Evidently, the maximum $|E_x|$ intensity under the grating ridge becomes much stronger than that under the grating trench as t decreases.

The coupling induced by another kind of near-field perturbation due to the variation of occupation ratio η is also explored fixing $t=20$ nm and $\Delta=200$ nm. It is observed from the absorption spectra in Fig. 3a that the resonant frequency blue-shifts from 15.84 to 18.18 THz continuously as η decreases

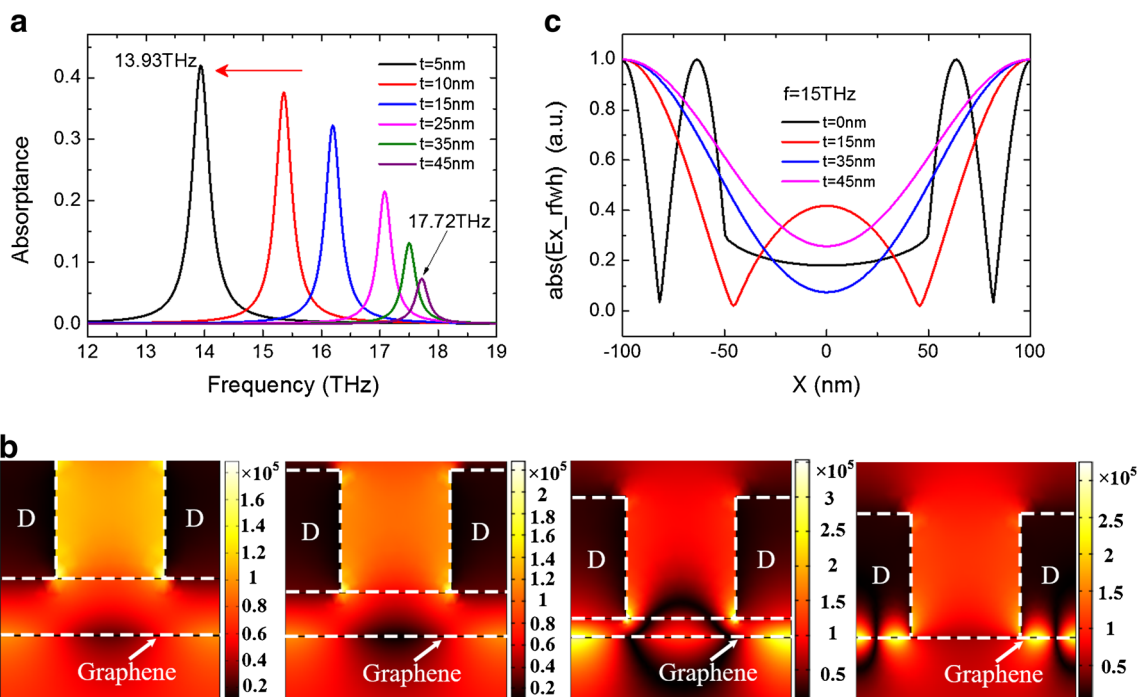


Fig. 2 a The evolution of the absorption spectra with varying distance t between the graphene and the dielectric grating when $\eta=50\%$ and $\Delta=200$ nm. **b** The variation of the electrical field distribution of the

fundamental GSP modes with a fixed frequency of 15 THz when $t=45, 35, 15,$ and 0 nm. **c** Normalized $|E_x|$ intensity on the graphene layer with different t

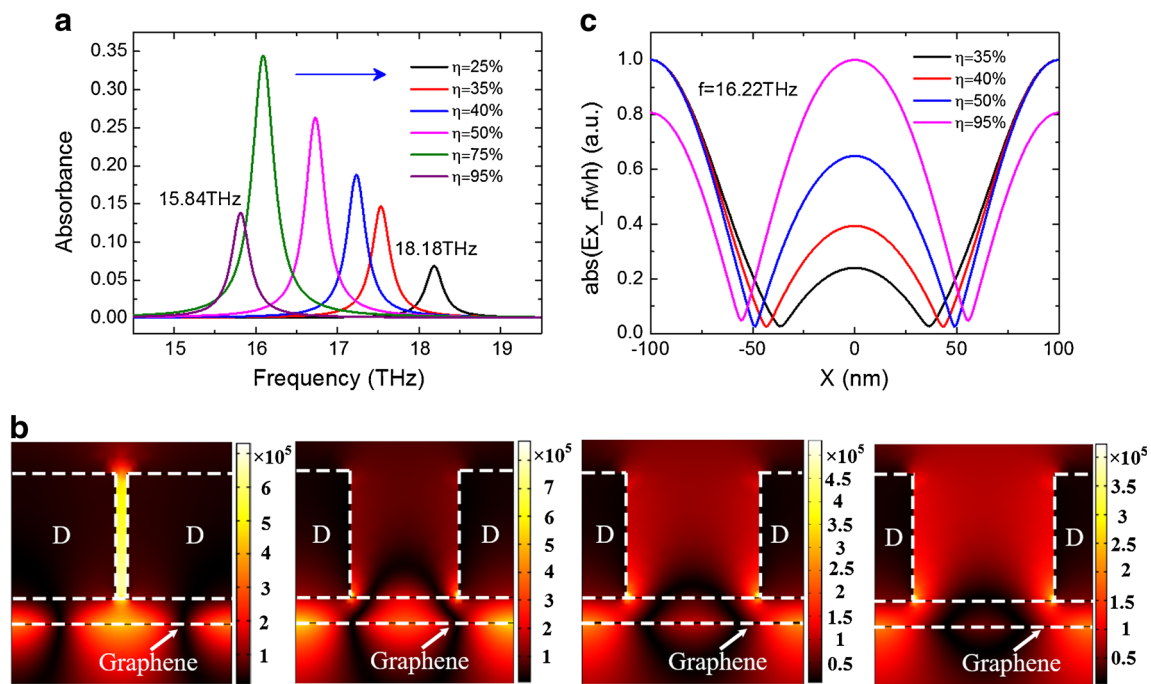


Fig. 3 **a** The evolution of the absorption spectra with different occupation ratio η in one dielectric grating period when $t=20$ nm and $\Lambda=200$ nm. **b** The variation of the electrical field distribution of the

fundamental mode with a fixed frequency of 16.22 THz when $\eta=95$, 50, 40, and 35 %. **c** Normalized $|E_x|$ intensity on the graphene layer with different η

from 95 to 25 %. However, the absorbance no longer varies monotonously; instead, it initially exhibits a sharp increasing behavior from only 13.12 % ($\eta=95$ %) to a maximum value of 41.97 % ($\eta=75$ %) and then decreasing to merely 6.9 % ($\eta=25$ %). This phenomenon indicates that the occupation ratio η of grating has a strong ability to modulate the absorbance of the hybrid system. Meanwhile, it is observed that the energy of GSP modes shows a concentration tendency toward the grating ridge as the occupation ratio η reduces (see Fig. 3b). This variation tendency can be further confirmed by Fig. 3c, which illustrates that the normalized $|E_x|$ at the point $X=0$ decreases from 0.98 to 0.21 as η decreases from 95 to 35 %.

Coupling of GSP Modes Induced by Perturbation in Metallic Nanostructure

Further investigation focuses on the effect of the near-field perturbation on the coupling between GSP modes and evanescent wave modes in the metallic grating. Simulations are performed using a gold grating with the same geometric parameters as the dielectric grating and the spacer with the same permittivity ($\epsilon_2=2.25$). Fig. 4a presents the absorption spectra with varying distance t between the metallic grating and the graphene. It illustrates that the shift of the resonant frequency of the MSGG hybrid system is approximately twice larger than that of the DGSG hybrid system. Meanwhile, the corresponding absorption efficiency is higher than that in the

DGSG hybrid system. These results indicate that the coupling effect between the GSP modes and evanescent wave modes in the MSGG hybrid system is stronger than that in the DGSG hybrid system.

In contrast to the DGSG hybrid system, a completely opposite feature is observed that the energy of the GSP mode under the ridge is gradually suppressed as the metallic grating approaches to the graphene, yielding a concentration of energy on the graphene layer under the grating gap instead of the ridge (displayed in Fig. 4b). Specially, when the grating contact with graphene directly ($t=0$), the GSP wave under the ridge is suppressed thoroughly. In the situation, as illustrated in Fig. 4c, the energy is mainly confined in the grating gap and the magnitude of $|E_x|$ at the metallic-graphene interface under the ridge is nearly zero.

Finally, we investigated the evolutions of the coupling behaviors when the occupation ratio η of metallic grating varies. It is found that the MSGG hybrid system still maintains a high absorbance even when its occupation ratio is large. As indicated in the absorption spectra in Fig. 5a, the absorbance of the MSGG hybrid system still remains at a high level (~ 49.1 %) when the occupation ratio η is larger than 75 %, while that of the DGSG hybrid system drops by a large margin to only 13.12 % (Fig. 3a). To further understand this behavior, the GSP modes profiles with varying η at 16.22 THz are visualized in Fig. 5b. Obviously, a surface plasmon wave with high intensity is generated in the grating gap when η equals 95 %, leading to a considerable confinement of the incident wave. In addition, as shown

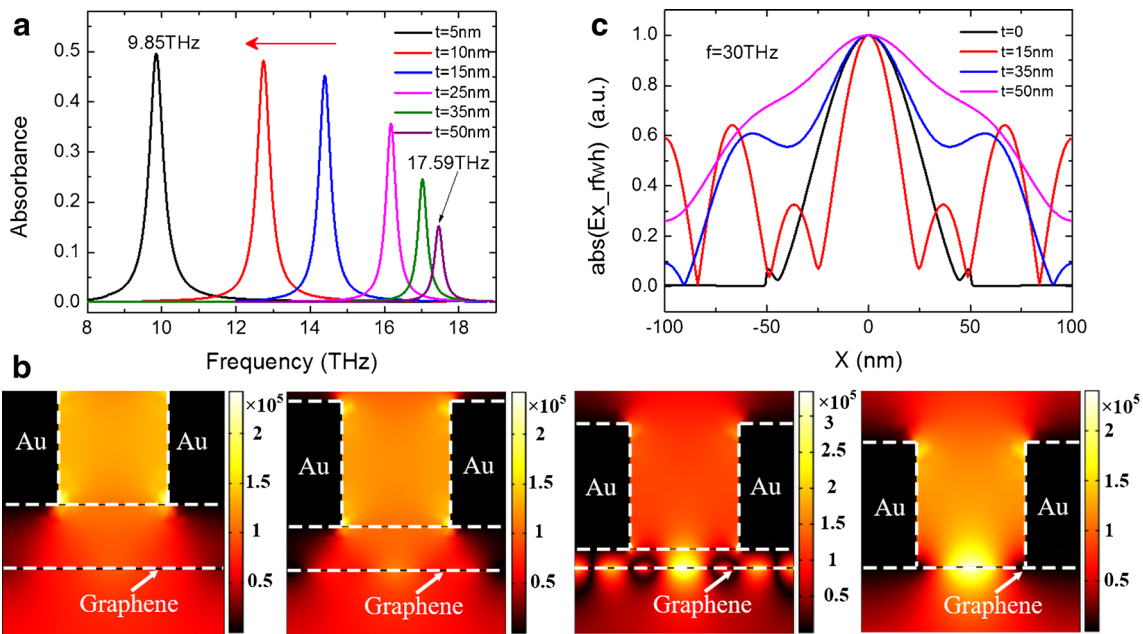


Fig. 4 **a** The evolution of the absorption spectra with varying distance t between the graphene and the metallic grating when $\eta=50\%$ and $\Lambda=200$ nm. **b** The variation of the electrical field distribution of the

fundamental mode with a fixed frequency of 30 THz when $t=50, 35, 15,$ and 0 nm. **c** Normalized $|Ex|$ intensity on the graphene layer with different t

in Fig. 5c, most portion of the two $|Ex|$ normalized intensity distribution curves when η equals 50 and 95 % are well overlapped, which means that a metallic grating with large

occupation ratio exhibits a stronger ability to modulate the incident light than a dielectric grating with the same geometry.

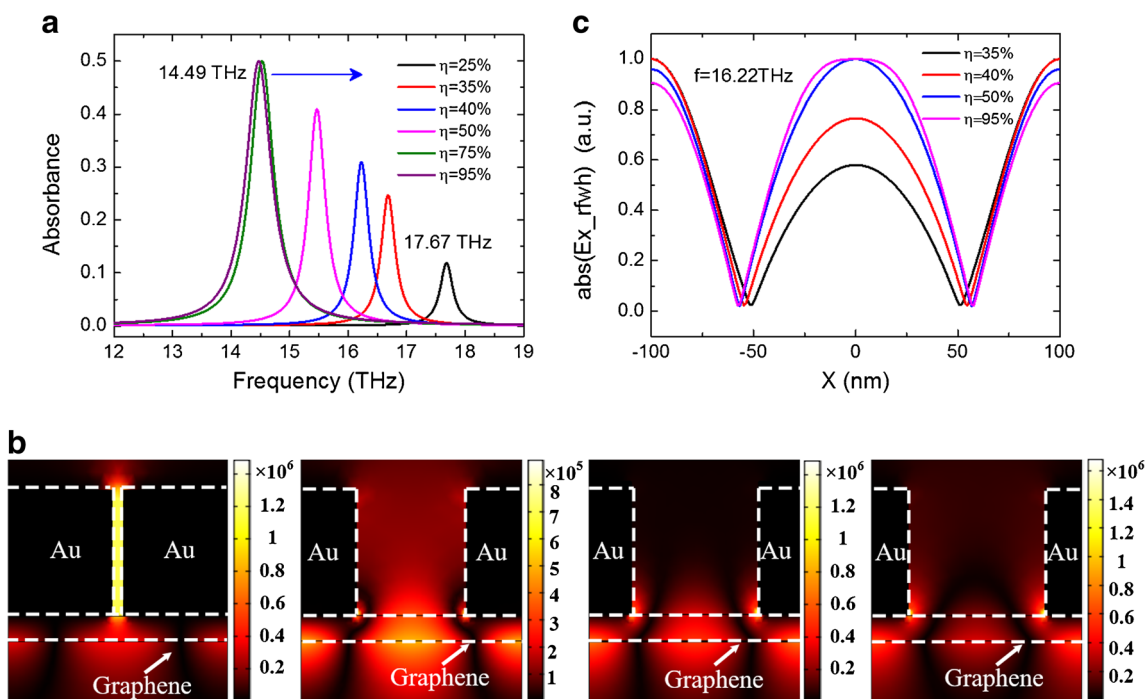


Fig. 5 **a** The evolution of the absorption spectra with different occupation ratio η in one metallic grating period when $t=20$ nm and $\Lambda=200$ nm. **b** The variation of the electrical field distribution of the

fundamental mode with a fixed frequency of 16.22 THz when $\eta=95, 50, 40,$ and 35% . **c** Normalized $|Ex|$ intensity on the graphene layer with different η

Physical Model and Mechanism

From the results presented above, it is clear that the coupling induced by the near-field perturbation results in the shift of the resonant frequency and the variation of absorbance. We first build a grating-spacer-graphene physical model to quantitatively unveil the shift of the resonant frequency using effective medium theory. For simplicity, we approximate the grating as an effective medium with relative permittivity of $\varepsilon_1 = [1 + \eta\varepsilon_r + (1 - \eta)\varepsilon_g]/2$ [30], where ε_r and ε_g are the permittivity of the grating ridge and the grating trench, respectively. In our considering terahertz frequencies, the conductivity of graphene is dominated by the intraband transitions, which can be represented by a Drude model [18]. The dispersion relation of GSP for TM modes in a continuous monolayer graphene in the hybrid system is approximately given by the following

$$q(\omega) = \frac{\pi\hbar^2\varepsilon_0(\varepsilon_3 + \bar{\varepsilon})}{e^2E_f} \left(1 + \frac{i}{\omega\tau}\right)\omega^2 \quad (1)$$

with $\bar{\varepsilon}$ defined as

$$\bar{\varepsilon} \equiv \varepsilon_2 \frac{(\varepsilon_1 + \varepsilon_2) \cdot \exp(2qt) + (\varepsilon_1 - \varepsilon_2)}{(\varepsilon_1 + \varepsilon_2) \cdot \exp(2qt) - (\varepsilon_1 - \varepsilon_2)}. \quad (2)$$

In Eq. 2, ω is the angular frequency of the incident light, e is the elementary charge, $\tau = 0.64$ ps is the relaxation time, \hbar is the reduced Planck's constant, $E_f = 0.1$ eV is the Fermi energy of graphene, and $\varepsilon_3 = 1$ is the permittivity of the background (air). In Eq. 3, $\bar{\varepsilon}$ is the permittivity of the spacer and grating when they are taken as an effective uniform medium, and ε_2 is the permittivity of the dielectric spacer. A GSP wave can be resonantly excited once the reciprocal lattice vectors of the grating matches the wave vectors of the GSP mode

$$Re[q(\omega)] = n \frac{2\pi}{\Lambda}, \quad (3)$$

where n is an integer and $n \cdot 2\pi/\Lambda$ is the reciprocal lattice vector of the grating. In this work, the plasmonic wave is excited by the first diffraction order, and hence $n = 1$ in Eq. 3. The resonant frequency ω_{GSP} can be expressed as

$$\omega_{\text{GSP}} = \sqrt{\frac{2e^2 \times E_f}{\hbar^2 \varepsilon_0 (\varepsilon_3 + \bar{\varepsilon}) \Lambda}}. \quad (4)$$

Based on the derivation above, the predicting resonant frequencies calculated using Eq. 4 with varying t and η are provided in Fig. 6a, b, respectively. Meanwhile, they are compared with the simulated results extracted from the absorption spectra in Fig. 2a, Fig. 3a, Fig. 4a, and Fig. 5a. One can clearly observe that the theoretical resonant frequencies show good agreement with the simulated ones. The shift of a resonant

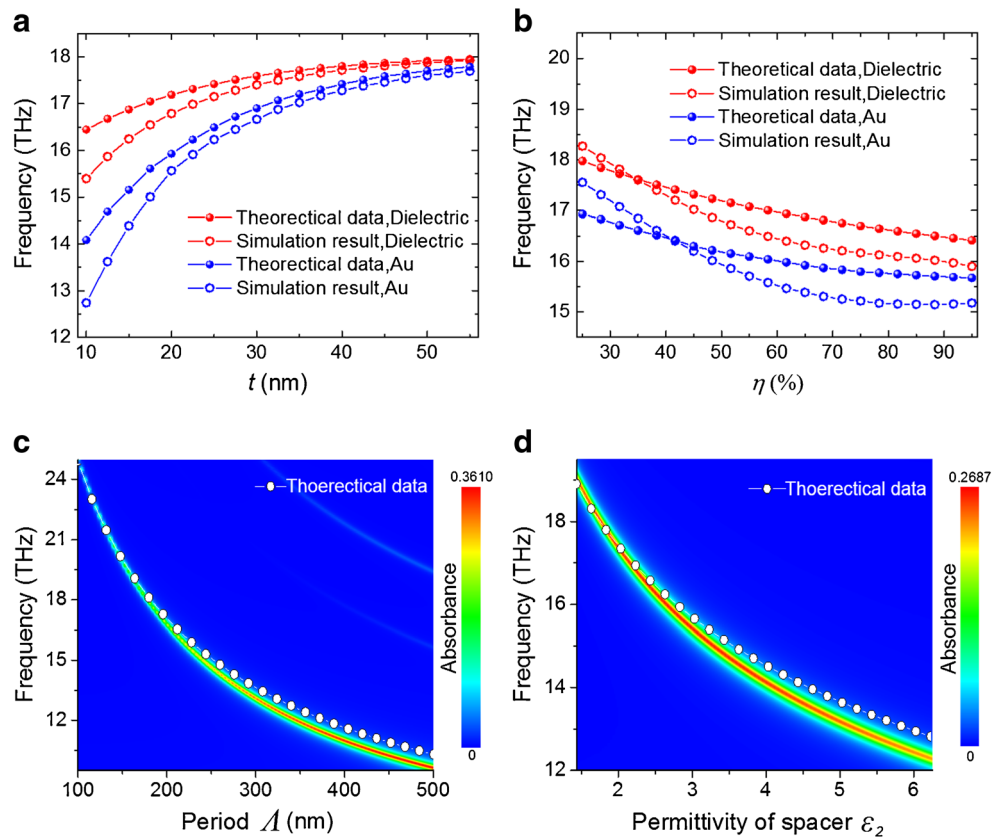
frequency is the result of the variation of the effective permittivity (i.e., Eq. 2) induced by the near-field perturbation. Specifically, the decrease of t (η) gives rise to the increase (decrease) of the effective permittivity around graphene, resulting in the redshift (blueshift) of resonant frequency. The effective medium physical model is further verified with varying grating period Λ and permittivity ε_2 of the spacer. The dependence of the absorption spectra of the DGSG hybrid system on Λ and ε_2 are calculated numerically and illustrated in Fig. 6c, d. The red light line represents the resonant frequency. One can visually see that the resonant frequency redshifts to the low frequency region as Λ and ε_2 increases due to the decrease of the effective permittivity around the graphene. Meanwhile, the analytical resonant frequencies are also calculated using Eq. 4 and shown as the white hollow sphere lines. Clearly, simulation results and theoretical ones are in well accordance. Therefore, our physical model is trustworthy in predicting the shift of the resonant frequency induced by the near-field perturbation in both two hybrid systems.

Besides, we revealed that the variation of absorbance in the coupling process is attributed to the change of the intensity of the first diffraction order in the grating. For the case when the distance t decreases, the coupling between the GSP modes and evanescent wave modes becomes stronger due to the exponential decay of intensity of the first diffraction order along the direction of the grating height (z -axis in Fig. 1a, b). This results in the monotonous increase of the absorbance (Fig. 2a and Fig. 4a). While for the case when η decreases, we find that the absorbance of the system is also modulated by the first diffraction order. In Fig. 7a, b, the intensity of the first diffraction order in both dielectric and metallic gratings are calculated using rigorous coupled wave theory and compared with the absorbance of the system. It shows that when the occupation ratio of the gratings increases, the absorbance exhibit a similar variation tendency with the intensity of the evanescent wave in both DGSG and MSGSG hybrid systems. This signifies that the absorbance of the hybrid systems is mainly determined by the intensity of the first order evanescent wave. We also note that the two curves in Fig. 7b exhibits slightly different tendency after the occupation ratio of metallic grating exceeds 60 %. This attributes to the fact that the absorbance is also dependent on the overlap area between the plasmonics mode and the evanescent wave mode [29], which varies slightly as the occupation ratio of metallic grating increases. The above quantitative revelation of the evolution of the spectra characteristics provides a guidance to design THz GSP devices with high-coupling efficiency.

Discussion

The above analysis has unveiled the evolution of the absorption spectra induced by the near-field perturbation. In this

Fig. 6 Comparison between theoretical resonant frequencies and simulation results with varying distance t (a) and occupation ratio η (b), respectively, when $\Lambda=200$ nm. **c** Simulated absorbance mapping of the DGSG hybrid system with varying grating period Λ and incident frequency. **d** Simulated absorbance mapping of the DGSG hybrid system with varying permittivity ϵ_2 of spacer and incident frequency when $t=20$ nm and $\eta=50\%$. The white hollow sphere lines are theoretical resonant frequencies as a function Λ and ϵ_2



section, we reveal the evolution of the GSP modes in such coupling process. We found that the opposite distribution tendency of the GSP mode energy in the hybrid systems as the grating approaches the graphene (Fig. 2b and Fig. 4b) is attributed to the different penetration abilities of GSP waves into the dielectric and metallic nano-gratings. To intuitively observe the penetration of the GSP wave into the grating, the GSP mode profiles of the DGSG and MSGS hybrid systems when $t=10$ nm, $\eta=50\%$, and $\Lambda=200$ nm are given in the insets in Fig. 8a, b, respectively, and the corresponding

normalized electric field amplitudes $|E_x|$ along the green lines (z -axis) are also extracted. For the DGSG hybrid system, $|E_x|$ first drops to 42 % at the spacer/dielectric interface (at the position of $Z=10$ nm), and then slowly falls to 35 % at the position of $Z=20$ nm in the dielectric grating. Whereas, $|E_x|$ rapidly reduces to only 1.5 % at the spacer/Au interface and becomes negligible at $Z=20$ nm in the MSGS hybrid system. These indicate that the GSP wave possesses a much stronger ability to penetrate into the dielectric grating than into the metallic grating.

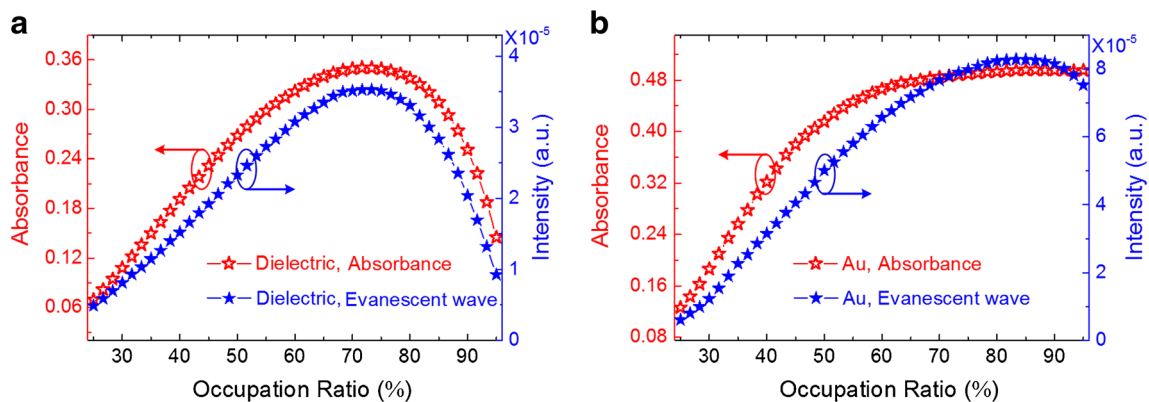
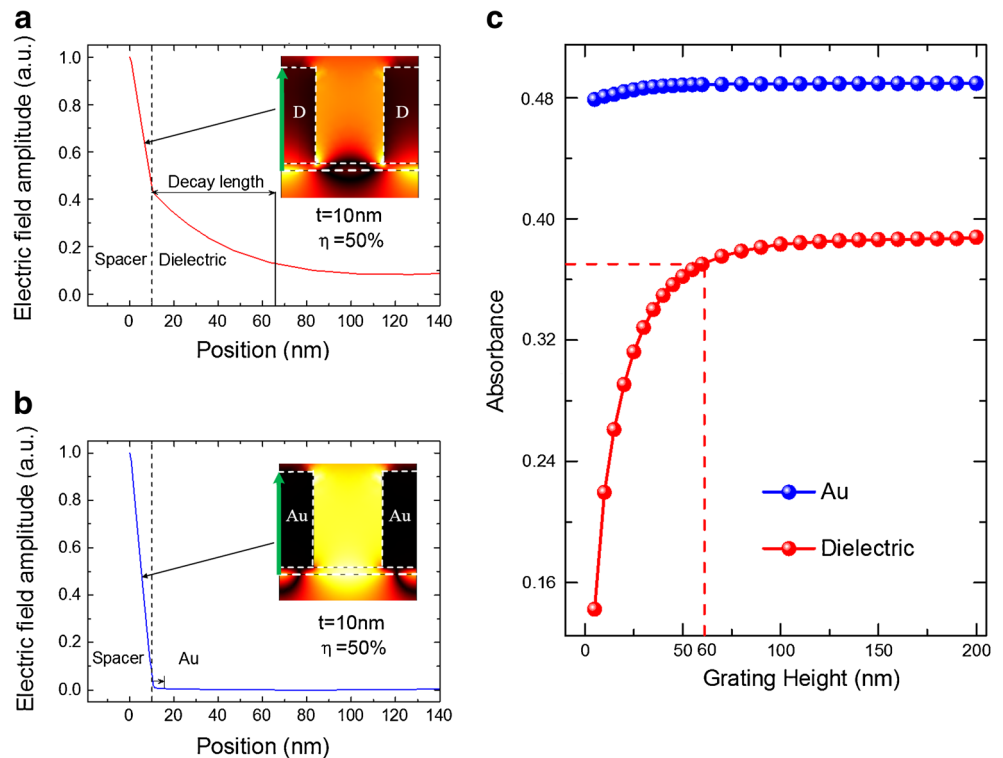


Fig. 7 Comparison between the numerical resonant absorbance and the first order evanescent wave intensities calculated by rigorous coupled wave theory in the hybrid systems with the occupation ratio η of the dielectric grating (a) and metallic grating (b) vary from 30 to 95 %. The

red hollow star lines represent the variation of the absorbance of the hybrid system while the blue solid star lines represent the variation of the intensity of the first order evanescent wave

Fig. 8 The distributions of electric field amplitudes along the green lines in the GSP modes for dielectric gratings (a) and Au gratings (b), respectively. c The dependence of the absorbance of the DGSG hybrid system and the MSGS hybrid system on grating heights h when it varies from 5 to 200 nm. Graphene is at the position of zero, dielectric and Au gratings are 10 nm away from graphene



To quantitatively measure the penetration ability, the decay length [21] into the nano-grating of a GSP wave is employed, which is defined as where the field amplitude drops to $1/e$ of that at the spacer/grating interface. According to this definition, the decay length of GSP waves in dielectric grating is ~ 60 nm as can be seen from Fig. 8a, which means the GSP wave can penetrate into the dielectric grating with a considerable length. Meanwhile, refractive index ($n_r=3.4$) of the grating ridge is larger than that of the grating gap ($n_g=1$) and the spacer ($n_{\text{spa}}=1.5$). Thus, the effective refractive index under the grating ridge increases as the grating approaches the graphene, resulting in the increase of the field intensity and a concentration tendency of GSP waves toward the grating ridge. On the other hand, the decay length of GSP waves in metallic grating is extremely small (only ~ 5 nm, see Fig. 8b), greatly suppressing the penetration of the GSP wave into the metallic grating; and hence, the GSP wave energy should concentrate to the grating gap instead of the grating ridge when the spacer thickness t is reduced. Especially for the case when the grating touches the graphene, the continuous GSP mode is completely suppressed at the metal-graphene interface, resulting in a localized mode confined in the grating gap. It means that in order to avoid localized GSP modes, we need to employ a dielectric spacer in the MSGS hybrid system. Based on these discussions, we can conclude that the different decay lengths of the GSP wave in the dielectric and metallic grating contribute to the opposite spatial energy distribution of GSP modes as the grating approaches the graphene.

In addition, we found that the different decay lengths of the GSP wave also determine the dependence of the absorbance of the hybrid systems on the grating height. We calculated the absorption spectra in both DGSG and MSGS system at different grating heights and extracted the resonant absorbance from the spectra. The results are shown in Fig. 8c. When h is larger than the decay length of GSP waves in dielectric grating (i.e., 60 nm), the resonant absorbance is nearly unchanged in the DGSG system. Nevertheless, when h is smaller than 60 nm, the energy of GSP wave cannot be completely confined in the system, and a portion of GSP wave is converted into free space wave, resulting in a sharp decay of the resonant absorbance to merely $\sim 10\%$ ($h=10$ nm). In contrast, for the MSGS hybrid system, its high absorbance barely changes even when h decreases to 5 nm, benefited from its extraordinary small decay length. This result indicates that the energy of GSP wave can be effectively trapped as long as the grating height is larger than the decay length, and the ultra-thin metallic grating exhibits stronger ability to confine and absorb the incident light than the ultra-thin dielectric grating.

The revealed penetration characteristics of GSP waves into dielectric and metallic grating promote innovative methods for controlling and confining terahertz wave. On one hand, the redistribution of GSP spatial energy in a sub-grating region offers a possible solution for ultra-high resolution imaging [31]; on the other hand, ultra-thin metal nanostructure with strong ability to confine the incident light allows for realizing the highly integration of three-dimensional stacked terahertz elements [32].

Conclusion

In conclusion, we systematically investigate the coupling effect between the GSP modes and evanescent wave modes induced by the near-field perturbation using finite element method. The underlying physical mechanism of the coupling effect is quantitatively revealed based on effective medium theory and the decisive factor that dominates the absorbance of the hybrid system is investigated using rigorous coupled wave theory, which exhibits good agreement with the simulated results. Furthermore, the redistribution and effective trapping of energy in the hybrid systems is found to be closely related to the penetration ability of the GSP wave into the nanostructure. These understandings facilitate further engineering of the next-generation GSP terahertz devices and system.

Acknowledgements This work is supported by the National High Technology Research and Development Program of China (2015AA034801), National Natural Science Foundation of China (No.61405021, 11374359), Specialized Research Fund for the Doctoral Program of Higher Education (20120191120021), Natural Science Foundation of Chongqing, China (cstc2014jcyjA40045), and the Fundamental Research Funds for the Central Universities (CDJZR12120004, 106112013CDJZR120006).

References

- Hong S-Y, Dadap JI, Petrone N, Yeh P-C, Hone J, Osgood RM (2013) Optical third-harmonic generation in graphene. *Physical Review X* 3(2):021014. doi:10.1103/PhysRevX.3.021014
- Koppens FH, Chang DE, Garcia de Abajo FJ (2011) Graphene plasmonics: a platform for strong light-matter interactions. *Nano letters* 11(8):3370–3377. doi:10.1021/nl201771h
- Chen J, Badioli M, Alonso-Gonzalez P, Thongrattanasiri S, Huth F, Osmond J, Spasenovic M, Centeno A, Pesquera A, Godignon P, Elorza AZ, Camara N, Garcia de Abajo FJ, Hillenbrand R, Koppens FH (2012) Optical nano-imaging of gate-tunable graphene plasmons. *Nature* 487(7405):77–81. doi:10.1038/nature11254
- Liu N, Mesch M, Weiss T, Hentschel M, Giessen H (2010) Infrared perfect absorber and its application as plasmonic sensor. *Nano letters* 10(7):2342–2348. doi:10.1021/nl9041033
- Mueller T, Xia F, Avouris P (2010) Graphene photodetectors for high-speed optical communications. *Nature Photonics* 4(5):297–301. doi:10.1038/nphoton.2010.40
- Willetts KA (2013) Super-resolution imaging of interactions between molecules and plasmonic nanostructures. *Phys Chem Chem Phys* 15(15):5345–5354. doi:10.1039/c3cp43882a
- You B, Peng CC, Jhang JS, Chen HH, Yu CP, Lai WC, Liu TA, Peng JL, Lu JY (2014) Terahertz plasmonic waveguide based on metal rod arrays for nanofilm sensing. *Opt Express* 22(9):11340–11350. doi:10.1364/OE.22.011340
- Ramanandan GKP, Adam AJL, Planken PCM (2014) Enhanced terahertz emission from schottky junctions using plasmonic nanostructures. *ACS Photonics* 1(11):1165–1172. doi:10.1021/ph500251a
- Vinnakota RK, Genov DA (2014) Terahertz optoelectronics with surface plasmon polariton diode. *Sci Rep* 4:4899. doi:10.1038/srep04899
- Grigorenko AN, Polini M, Novoselov KS (2012) Graphene plasmonics. *Nat Photonics* 6(11):749–758. doi:10.1038/nphoton.2012.262
- Low T, Avouris P (2014) Graphene plasmonics for terahertz to mid-infrared applications. *ACS Nano* 8(2):1086–1101. doi:10.1021/nn406627u
- Yan H, Low T, Zhu W, Wu Y, Freitag M, Li X, Guinea F, Avouris P, Xia F (2013) Damping pathways of mid-infrared plasmons in graphene nanostructures. *Nat Photonics* 7(5):394–399. doi:10.1038/nphoton.2013.57
- Jablan M, Buljan H, Soljačić M (2009) Plasmonics in graphene at infrared frequencies. *Physical Review B* 80 (24):245435. doi:10.1103/PhysRevB.80.245435
- Fei Z, Rodin AS, Andreev GO, Bao W, McLeod AS, Wagner M, Zhang LM, Zhao Z, Thiemens M, Dominguez G, Fogler MM, Castro Neto AH, Lau CN, Keilmann F, Basov DN (2012) Gate-tuning of graphene plasmons revealed by infrared nano-imaging. *Nature* 487(7405):82–85. doi:10.1038/nature11253
- Zhu X, Yan W, Uhd Jepsen P, Hansen O, Asger Mortensen N, Xiao S (2013) Experimental observation of plasmons in a graphene monolayer resting on a two-dimensional subwavelength silicon grating. *Appl Phys Lett* 102(13):131101. doi:10.1063/1.4799173
- Fang Z, Wang Y, Schlather AE, Liu Z, Ajayan PM, Garcia de Abajo FJ, Nordlander P, Zhu X, Halas NJ (2014) Active tunable 002-absorption enhancement with graphene nanodisk arrays. *Nano letters* 14(1):299–304. doi:10.1021/nl404042h
- Li H-J, Wang L-L, Liu J-Q, Huang Z-R, Sun B, Zhai X (2013) Investigation of the graphene based planar plasmonic filters. *Appl Phys Lett* 103(21):211104. doi:10.1063/1.4831741
- Chu H-S, How Gan C (2013) Active plasmonic switching at mid-infrared wavelengths with graphene ribbon arrays. *Appl Phys Lett* 102(23):231107. doi:10.1063/1.4810003
- Nikitin AY, Guinea F, Martin-Moreno L (2012) Resonant plasmonic effects in periodic graphene antidot arrays. *Appl Phys Lett* 101(15):151119. doi:10.1063/1.4760230
- Sreekanth KV, Zeng S, Shang J, Yong KT, Yu T (2012) Excitation of surface electromagnetic waves in a graphene-based Bragg grating. *Sci Rep* 2:737. doi:10.1038/srep00737
- Gao W, Shu J, Qiu C, Xu Q (2012) Excitation of plasmonic waves in graphene by guided-mode resonances. *ACS Nano* 6(9):7806–7813. doi:10.1021/nn301888e
- Chen L, Zhang T, Li X, Wang G (2013) Plasmonic rainbow trapping by a graphene monolayer on a dielectric layer with a silicon grating substrate. *Opt Express* 21(23):28628–28637. doi:10.1364/OE.21.028628
- Tang L, Du J, Du C, Zhu P, Shi H (2014) Scaling phenomenon of graphene surface plasmon modes in grating-spacer-graphene hybrid systems. *Opt Express* 22(17):20214–20222. doi:10.1364/OE.22.020214
- Wang B, Zhang X, Yuan X, Teng J (2012) Optical coupling of surface plasmons between graphene sheets. *Appl Phys Lett* 100(13):131111. doi:10.1063/1.3698133
- Capmany J, Domenech D, Muñoz P (2014) Silicon graphene waveguide tunable broadband microwave photonics phase shifter. *Opt Express* 22(7):8094. doi:10.1364/oe.22.008094
- Auditoro A, de Angelis C, Locatelli A, Aceves AB (2013) Tuning of surface plasmon polaritons beat length in graphene directional couplers. *Opt Express* 38(20):4228–4231. doi:10.1364/OL.38.004228
- Raman A, Fan S (2011) Perturbation theory for plasmonic modulation and sensing. *Phys Rev B* 83:20. doi:10.1103/PhysRevB.83.205131
- Ordal MA, Bell RJ, Alexander RW, Long LL, Querry MR (1985) Optical properties of fourteen metals in the infrared and far infrared: Al, Co, Cu, Au, Fe, Pb, Mo, Ni, Pd, Pt, Ag, Ti, V, and W. *Appl Optics* 24(24):4493–4499. doi:10.1364/AO.24.004493

29. A Y (1973) Coupled-mode theory for guided-wave optics. *IEEE Journal of Quantum Electronics* 9 (9):919–933. doi:[10.1109/JQE.1973.1077767](https://doi.org/10.1109/JQE.1973.1077767)
30. Peres NM, Bludov YV, Ferreira A, Vasilevskiy MI (2013) Exact solution for square-wave grating covered with graphene: surface plasmon-polaritons in the terahertz range. *J Phys Condens Matter: an Inst of Phys J* 25(12):125303. doi:[10.1088/0953-8984/25/12/125303](https://doi.org/10.1088/0953-8984/25/12/125303)
31. Li P, Taubner T (2012) Broadband subwavelength imaging using a tunable graphene-lens. *ACS Nano* 6(11):10107–10114
32. Yan H, Li X, Chandra B, Tulevski G, Wu Y, Freitag M, Zhu W, Avouris P, Xia F (2012) Tunable infrared plasmonic devices using graphene/insulator stacks. *Nat Nanotechnol* 7(5):330–334. doi:[10.1038/nnano.2012.59](https://doi.org/10.1038/nnano.2012.59)